11-2015

Pharmacological Modulation of Photoreceptor Outer Segment Degradation in a Human iPS Cell Model of Inherited Macular Degeneration

Ruchira Singh
University of Wisconsin-Madison

David Kuai
University of Wisconsin-Madison

Karina E. Guziewicz
University of Pennsylvania, karinag@vet.upenn.edu

Jackelyn Meyer
University of Wisconsin-Madison

Molly Wilson
University of Wisconsin-Madison

See next page for additional authors

Pharmacological Modulation of Photoreceptor Outer Segment Degradation in a Human iPS Cell Model of Inherited Macular Degeneration

Abstract
Degradation of photoreceptor outer segments (POS) by retinal pigment epithelium (RPE) is essential for vision, and studies have implicated altered POS processing in the pathogenesis of some retinal degenerative diseases. Consistent with this concept, a recently established hiPSC-RPE model of inherited macular degeneration, Best disease (BD), displayed reduced rates of POS breakdown. Herein we utilized this model to determine (i) if disturbances in protein degradation pathways are associated with delayed POS digestion and (ii) whether such defect(s) can be pharmacologically targeted. We found that BD hiPSC-RPE cultures possessed increased protein oxidation, decreased free-ubiquitin levels, and altered rates of exosome secretion, consistent with altered POS processing. Application of valproic acid (VPA) with or without rapamycin increased rates of POS degradation in our model, whereas application of bafilomycin-A1 decreased such rates. Importantly, the negative effect of bafilomycin-A1 could be fully reversed by VPA. The utility of hiPSC-RPE for VPA testing was further evident following examination of its efficacy and metabolism in a complementary canine disease model. Our findings suggest that disturbances in protein degradation pathways contribute to the POS processing defect observed in BD hiPSC-RPE, which can be manipulated pharmacologically. These results have therapeutic implications for BD and perhaps other maculopathies.

Disciplines
Medicine and Health Sciences | Veterinary Medicine

Author(s)
Ruchira Singh, David Kuai, Karina E. Guziewicz, Jackelyn Meyer, Molly Wilson, Jianfeng Lu, Molly Smith, Eric Clark, Amelia Verhoeven, Gustavo D. Aguirre, and David M. Gamm

Pharmacological Modulation of Photoreceptor Outer Segment Degradation in a Human iPS Cell Model of Inherited Macular Degeneration

Ruchira Singh[1,2], David Kuai[1], Karina E Guziewicz[3] Jackelyn Meyer[1], Molly Wilson[1], Jianfeng Lu[1], Molly Smith[1], Eric Clark[1], Amelia Verhoeven[1], Gustavo D Aguirre[3] and David M Gamm[1,2,4]

[1]Waisman Center, University of Wisconsin-Madison, Madison, Wisconsin, USA; [2]McPherson Eye Research Institute, University of Wisconsin, Madison, Wisconsin, USA; [3]Department of Clinical Studies-Philadelphia, School of Veterinary Medicine, University of Pennsylvania, Philadelphia, Pennsylvania, USA; [4]Department of Ophthalmology and Visual Sciences, University of Wisconsin, Madison, Wisconsin, USA

Degradation of photoreceptor outer segments (POS) by retinal pigment epithelium (RPE) is essential for vision, and studies have implicated altered POS processing in the pathogenesis of some retinal degenerative diseases. Consistent with this concept, a recently established hiPSC-RPE model of inherited macular degeneration, Best disease (BD), displayed reduced rates of POS breakdown. Herein we utilized this model to determine (i) if disturbances in protein degradation pathways are associated with delayed POS digestion and (ii) whether such defect(s) can be pharmacologically targeted. We found that BD hiPSC-RPE cultures possessed increased protein oxidation, decreased free-ubiquitin levels, and altered rates of exosome secretion, consistent with altered POS processing. Application of valproic acid (VPA) with or without rapamycin increased rates of POS degradation in our model, whereas application of bafilomycin-A1 decreased such rates. Importantly, the negative effect of bafilomycin-A1 could be fully reversed by VPA. The utility of hiPSC-RPE for VPA testing was further evident following examination of its efficacy and metabolism in a complementary canine disease model. Our findings suggest that disturbances in protein degradation pathways contribute to the POS processing defect observed in BD hiPSC-RPE, which can be manipulated pharmacologically. These results have therapeutic implications for BD and perhaps other maculopathies.

Received 27 April 2015; accepted 23 July 2015; advance online publication 1 September 2015. doi:10.1038/mt.2015.141

INTRODUCTION

Macular degenerative diseases (MDDs) are a complex group of disorders that comprise a major cause of blindness worldwide. Dysfunction of retinal pigment epithelium (RPE) cells leading to loss of photoreceptors occurs in a number of MDDs, including age-related macular degeneration (AMD). In many of these MDDs, accumulation of partially digested photoreceptor outer segment (POS) products in RPE cells, possibly due to disturbances in protein degradation, has been implicated in disease progression.[1–4]

POS are taken up by RPE cells as phagosomes, which fuse with lysosomes to create phagolysosomes that are capable of degrading their cargo.[5,6] A recent study has demonstrated a role for noncanonical autophagy in the POS degradation process as well.[7] Coordination of POS degradation, proteolysis, and release of cellular waste products by RPE cells requires a collaborative effort between the proteasome, lysosome, autophagy, and exocytotic pathways. In corroboration of this concept, alterations in the cellular ubiquitin-proteasome system (UPS) and exocytosis have been associated with MDD pathophysiology,[8–12] and a single nucleotide variation in ubiquitin ligase (UBE3D) was recently linked to an increased incidence of AMD.[12]

To date, the role of protein degradation pathways in RPE physiology and MDD has largely been deciphered using genetically engineered mouse models, cultured human fetal RPE, and transformed RPE cell lines (ARPE19) exposed to oxidative stressors.[9,11,13–15] Human induced pluripotent stem cells (hiPSCs) offer a particularly attractive platform to interrogate disease pathophysiology using a patient's own cells, thus increasing the likelihood that they recapitulate important disease mechanisms. hiPSC-derived disease model systems also permit manipulation of cellular environment, and thus are conducive to drug testing. Importantly for such studies, we and others have shown that hPSC-RPE demonstrates key physical and functional attributes of mature RPE *in vivo*.[16–25]

We recently developed a patient-derived hiPSC-RPE model of Best disease (BD), a slowly progressive, untreatable form of MDD with autosomal dominant inheritance. BD hiPSC-RPE displayed delayed RHODOPSIN (RHO) degradation and increased accumulation of autofluorescent material after POS feeding.[2] As such, this BD hiPSC-RPE model offers a unique opportunity to investigate protein degradation pathways and search for drugs that affect the rate of POS degradation in patient-derived RPE.

In the current study, we show that in addition to POS handling defects, BD hiPSC-RPE displays increased baseline levels of oxidized proteins, decreased free-ubiquitin levels, and an elevated rate of exocytosis, suggesting that perturbations in protein degradation

Correspondence: David M. Gamm, T609 Waisman Center, University of Wisconsin School of Medicine and Public Health, 1500 Highland Avenue, Madison, Wisconsin 53705, USA. E-mail: dgamm@wisc.edu

pathways contribute to disease pathophysiology. Furthermore, we demonstrate that the BD phenotype can be partially mimicked in control hiPSC-RPE by treatment with BafA1, a V-ATPase inhibitor that inhibits autophagy and lysosomal function.[26,27] Conversely, the US Food and Drug Administration (FDA)–approved HDAC inhibitor valproic acid (VPA) increased the kinetics of POS breakdown in both control and BD hiPSC-RPE. Combinatorial drug therapy consisting of VPA and the autophagy inducer rapamycin (RAPA)[28] was even more effective in increasing the rate of POS degradation in BD hiPSC-RPE. Early treatment of a canine model of autosomal recessive BD with VPA yielded promising results; however, serum studies revealed that dogs rapidly metabolize VPA, limiting their utility for testing this drug. These findings have therapeutic implications for the treatment of BD and other maculopathies where defective POS handling instigates or exacerbates MDD progression. In addition, our study presents a scenario in which a hiPSC model system may be a useful option for testing drug efficacy when available animal models are suboptimal.

RESULTS

Accumulation of POS-derived autofluorescent material and increased baseline carbonylated protein content in BD hiPSC-RPE

Two hiPSC lines were derived from each of two BD patients with missense mutations in BEST1 (BD-1: A146K; BD-2: N296H) and their unaffected sibling controls (Ctr-1: sibling of BD-1; Ctr-2: sibling of BD-2).[2] RPE differentiated from these hiPSC lines displayed reproducible, characteristic cobblestone morphology and pigmentation (**Figure 1a**). Furthermore, when challenged with chronic daily POS feeding (1.5 months) followed by 15 days of consecutive washes without POS exposure, BD hiPSC-RPE showed increased accumulation of autofluorescent material compared to hiPSC-RPE derived from sibling controls (representative images from Ctr-1 and BD-1, **Figure 1b**, representative images from Ctr-2 and BD-2, **Supplementary Figure S1A**), confirming previous findings.[2] No autofluorescence was observed in control or BD hiPSC-RPE in the absence of POS feeding (data not shown). Given that cellular health, oxidative stress, and impaired proteolytic degradation have been linked to the accumulation of autofluorescent waste material in postmitotic cells,[13,14,29,30] we next investigated the levels of carbonylated proteins and oxidative stress modulators in control versus BD hiPSC-RPE cells. In the absence of POS feeding, the amount of oxidized proteins in BD hiPSC-RPE was higher relative to control hiPSC-RPE (BD-1 versus Ctr-1: 3.16 ± 0.90-fold, $P = 0.055$; BD-2 versus Ctr-2: 4.56 ± 1.19-fold, $P < 0.05$; **Figure 1c**). However, there were no clear differences in the relative expression of oxidative stress genes between control and BD hiPSC-RPE (**Figure 1d**; **Supplementary Table S1**). The finding of increased oxidized protein levels in the absence of overt free radical stress implicates impaired protein degradation as a possible component of the baseline cellular pathophysiology in BD hiPSC-RPE, as well as a contributor to the altered POS degradation kinetics seen in this model.[2]

Altered POS protein degradation, proteasomal function, and exocytosis in BD hiPSC-RPE

In experiments aimed at identifying pathways involved in the POS handling defect in BD hiPSC-RPE, control and mutant hiPSC-RPE were fed unlabeled POS (~20 POS/RPE cell) for 2 hours, and the amount of intracellular RHO, the most abundant protein component of POS, was quantified at 0, 4, 24, 48, and 120 hours postfeeding (representative images from Ctr-2 and BD-2, **Figure 2a**).[16] BD hiPSC-RPE always showed delayed degradation of ingested POS compared to control hiPSC-RPE, with RHO protein present in BD hiPSC-RPE at the 24, 48, and 120 hour time points (**Figure 2a**). Delayed degradation of RHO in BD hiPSC-RPE was further pronounced when control and mutant hiPSC-RPE were fed ~50 POS/RPE cell (**Supplementary Figure S1B**).[16] Similar to our previously published study, no consistent difference in the uptake of POS was seen between BD hiPSC-RPE and control hiPSC-RPE,[16] although we occasionally observed less RHO at 0 hour in the BD group.

Given that BD hiPSC-RPE showed delayed degradation of POS, we next investigated whether general intracellular protein turnover was affected in BD hiPSC-RPE. We focused first on the proteasomal pathway since it plays an essential role in the removal of misfolded and oxidized proteins,[31–33] and levels of the latter were elevated in BD hiPSC-RPE (**Figure 1c**). Proteasomal activity, measured by a chymotrypsin-like cell-based assay, was similar in BD versus control hiPSC-RPE (BD-1 versus Ctr-1: 1.34 ± 0.43-fold; BD-2 versus Ctr-2: 1.11 ± 0.21-fold; **Supplementary Figure S2A**). Furthermore, immunocytochemical analysis did not reveal any difference in the localization and expression of ubiquitin (UB) between control and BD hiPSC-RPE (**Figure 2b**). However, the protein level of free-UB was lower in BD-2 versus Ctr-2 hiPSC-RPE (0.68 ± 0.12-fold, $P = 0.04$; **Figure 2c,d and Supplementary Figure S2B**). Decreased levels of free-UB were also consistently observed between BD-1 and Ctr-1 hiPSC-RPE, but this difference did not reach statistical significance when averaged across multiple experiments (**Figure 2c and Supplementary Figure S2B,C**). In contrast, no difference in the amount of poly-UB proteins was seen between BD and control hiPSC-RPE (BD-1 versus Ctr-1: 1.05 ± 0.05-fold; BD-2 versus Ctr-2: 1.06 ± 0.03-fold; **Figure 2d** and **Supplementary Figure S2C**).

Exocytosis also plays an important role in protein trafficking by regulating the release of waste products from the cell, and has been shown to be altered in normal retinal aging and AMD.[9,34] Indeed, drusen deposits characteristically found in patients with AMD show high levels of the exosome proteins CD63 and LAMP2.[9,34] Following validation of our exosome isolation protocol using the exosome marker CD63 (**Supplementary Figure S3A,B**), media was collected from the apical and basal chambers of transwells containing monolayers of RPE. Thereafter, quantification of total protein revealed increased secretion of exosomes on both the apical and basal sides of BD hiPSC-RPE relative to control cultures (BD-2 versus Ctr-2 apical: 2.12 ± 0.52-fold, $P = 0.06$ and basal: 1.49 ± 0.23-fold, $P < 0.05$; BD-1 versus Ctr-1 apical: 2.13 ± 0.23, $P = 0.008$ and basal: 1.16 ± 0.04, P value not significant; **Figure 2e**). Subsequent comparisons demonstrated higher levels of CD63 in apically and basally secreted exosomes collected from BD versus control hiPSC-RPE (**Figure 2f**). Ponceau staining of western blot membranes also revealed higher levels of total protein in exosome samples collected from apical and basal media of BD versus control hiPSC-RPE (**Supplementary Figure S3C**). Together, these results suggest

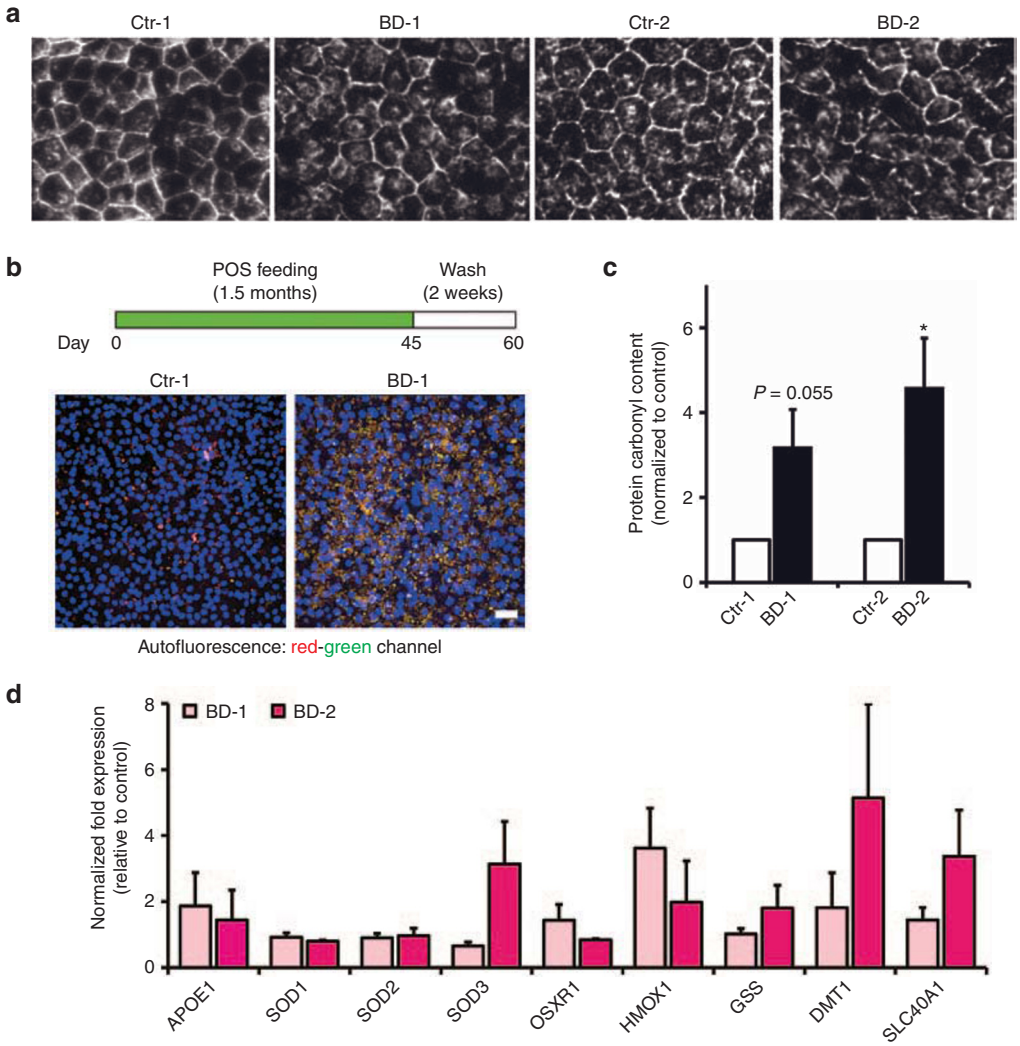

Figure 1 Accumulation of POS-derived autofluorescent material and oxidized proteins in BD hiPSC-RPE. (**a**) Representative light microscopic images of control and BD hiPSC-RPE (Ctr-1: sibling of BD-1; Ctr-2: sibling of BD-2). (**b**) Control and BD hiPSC-RPE were fed POS daily for 1–1.5 months followed by daily washes for two weeks. Representative confocal microscopic images showing accumulation of autofluorescent (red and green channels) material in Ctr-1 and BD-1 hiPSC-RPE. (**c**) Baseline carbonylated protein levels in BD hiPSC-RPE normalized to respective control hiPSC-RPE cultures. (**d**) Expression of genes associated with oxidative stress in BD hiPSC-RPE cultures normalized to their respective controls. Bars = 50 µm. *$P < 0.05$. BD, Best disease; hiPSC, human induced pluripotent stem cell; POS, photoreceptor outer segment; RPE, retinal pigment epithelium.

that perturbations in proteolytic pathways could contribute to the delayed POS degradation seen in BD hiPSC-RPE, with enhanced exocytosis occurring as a possible compensatory response to combat retained intracellular waste.

Examination of autophagy and lysosomal function in BD hiPSC-RPE

Given that ubiquitination can also modulate autophagy-mediated protein breakdown,[35] and both autophagy and lysosomal function play an important role in POS phagocytosis and degradation in RPE cells,[7,15,36] we next looked at the expression and localization of key proteins and enzymes in these two pathways. No difference in the protein expression of LC3 I or LC3 II, or in the LC3 II/I ratio, was observed between BD and control hiPSC-RPE (BD-1 versus Ctr-1: 1.01 ± 0.23; BD-2 versus Ctr-2: 0.78 ± 0.30; **Figure 3a,b**). Furthermore, no differences in the expression of P62 (also called SQSTM1), a marker of autophagic flux, or BECN1, an autophagy modulator, were seen between BD and control hiPSC-RPE (P62, BD-1 versus Ctr-1: 0.99 ± 0.22-fold; BD-2 versus Ctr-2: 1.12 ± 0.09-fold; BECN1, BD-2 versus Ctr-2: 1.32 ± 0.33-fold; **Supplementary Figures S4A,B** and **S5A,B**). Localization of the lysosomal protein LAMP1 by immunocytochemistry was also similar between BD and control hiPSC-RPE (**Figure 3c**), as was the protein expression of both LAMP1 and LAMP2 (LAMP1, BD-1 versus Ctr-1: 1.19 ± 0.13-fold; BD-2 versus Ctr-2: 0.76 ± 0.08-fold; LAMP2, BD-1 versus Ctr-1: 1.33 ± 0.04-fold; BD-2 versus Ctr-2: 0.98 ± 0.05-fold; **Figure 3c** and **Supplementary Figures S4C** and **S5C,D**). Western blot and immunohistochemical analyses of CTSD, a lysosomal enzyme involved in POS degradation by RPE,[37,38] and CTSB revealed no differences in their localization and expression between BD and control hiPSC-RPE (CTSD, BD-1 versus Ctr-1: 0.91 ± 0.06-fold; BD-2 versus Ctr-2: 0.91 ± 0.05-fold; CTSB, BD-1 versus Ctr-1: 1.33 ± 0.04-fold; BD-2 versus Ctr-2: 0.98 ± 0.05-fold; **Figure 3d** and **Supplementary Figure S5E,F**).

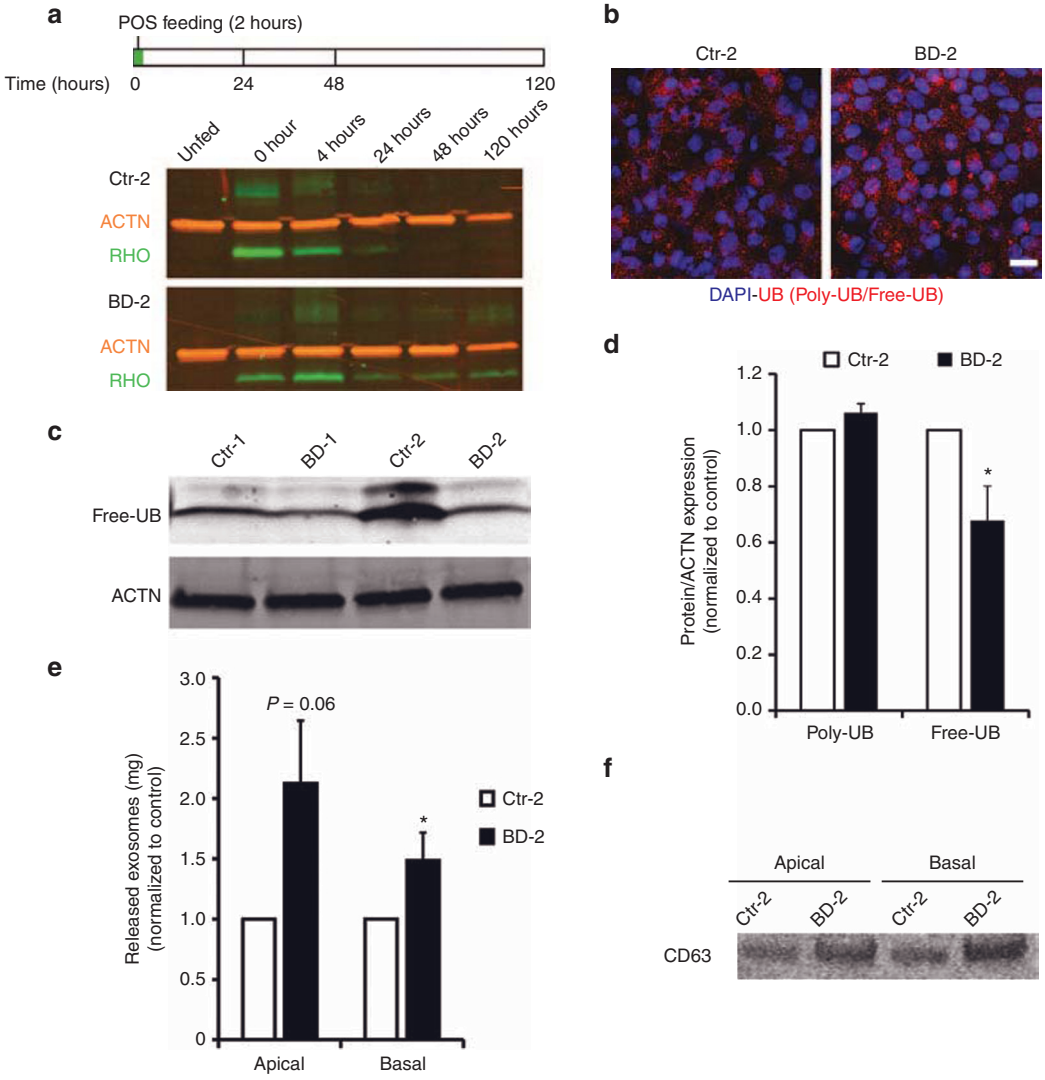

Figure 2 Comparison of POS degradation, proteasome function, and exosome secretion in control versus BD hiPSC-RPE. (**a**) Schematic (upper panel) depicting the protocol used to assess uptake and degradation of the POS-specific protein, RHO, in hiPSC-RPE. Western blot analysis (lower panel) showing the amount of RHO present in Ctr-2 versus BD-2 hiPSC-RPE at 0, 4, 24, 48, and 120 hours after 2 hour POS feeding (20 POS/RPE cell). (**b**) Confocal microscopic image showing the localization of total UB protein (poly-UB + free-UB) in Ctr-2 and BD-2 hiPSC-RPE. (**c**,**d**) Representative western blot image (**c**) and quantification (**d**) of free-UB and poly-UB in control versus BD hiPSC-RPE. Data in panel **d** is expressed as a fraction of free-UB or poly-UB relative to ACTIN (ACTN) in each sample, normalized to control hiPSC-RPE. (**e**) Quantification of exosome release from Ctr-2 versus BD-2 hiPSC-RPE into apical and basal media. (**f**) Western blot comparing CD63 levels in exosome samples isolated from the apical and basal media of Ctr-2 and BD-2 hiPSC-RPE. Bar = 20 µm. ACTN = ACTIN control. *$P < 0.05$. BD, Best disease; DAPI, 4′,6-diamidino-2-phenylindole; hiPSC, human induced pluripotent stem cell; POS, photoreceptor outer segment; RHO, RHODOPSIN; RPE, retinal pigment epithelium; UB, ubiquitin.

Lastly, we assessed lysosomal pH in hiPSC-RPE using a commercially available dye, lysosensor yellow-blue. As with the aforementioned experiments, no difference in baseline lysosomal pH was seen in BD versus control hiPSC-RPE (BD-1: 4.25 ± 0.08 versus Ctr-1: 4.38 ± 0.10; BD-2: 4.82 ± 0.10 versus Ctr-2: 4.87 ± 0.11; **Supplementary Figure S4D**). As a control, we measured lysosomal pH in human fetal RPE, hfRPE, (4.91 ± 0.01) in the presence or absence of the alkalinizing agent chloroquine, which significantly increased lysosomal pH (to 5.44 ± 0.18; **Supplementary Figure 4D**). Based on these results, there appears to be no detectable dysfunction of autophagy or lysosomal protein degradation pathways in our BD hiPSC-RPE models.

Modulation of POS degradation in hiPSC-RPE

If altered protein degradation contributes to the delay in POS breakdown observed in BD hiPSC-RPE, we should be able to mimic this POS processing defect in normal hiPSC-RPE by targeting protein degradation pathways. Control hiPSC-RPE cells were treated with bafilomycin A1 (BafA1), a V-ATPase inhibitor that affects autophagosome-lysosome fusion,[26,27] and then fed unlabeled POS for 2 hours. After washing, the amount of RHO protein present in the hiPSC-RPE cells was quantified by Western blot analysis at 0 and 24 hours (**Figure 4a**). No difference was observed in RHO levels between untreated and BafA1-treated control hiPSC-RPE at 0 h (lane 1 versus lane 2). However, at the

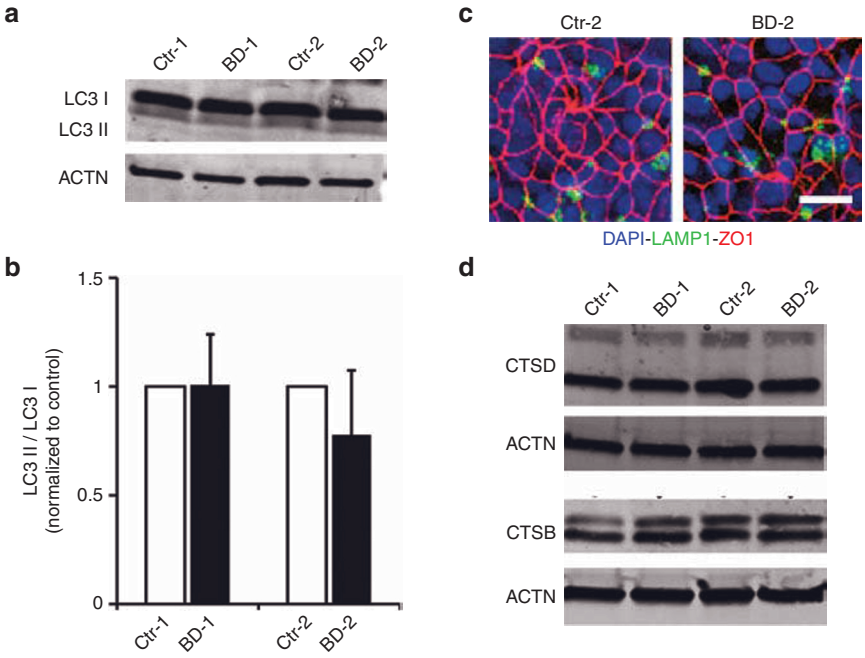

Figure 3 Expression and localization of autophagy and lysosomal proteins in control versus BD hiPSC-RPE. (**a,b**) Representative western blot image (**a**) and quantification (**b**) showing expression levels of the autophagy markers LC3 I and LC3 II and the LC3 II/I ratio in BD hiPSC-RPE normalized to their respective control hiPSC-RPE. (**c**) Localization of the lysosomal protein LAMP1 (green) and the tight junction protein ZO-1 (red) by confocal microscopy in Ctr-2 and BD-2 hiPSC-RPE. (**d**) Western blot analyses comparing the expression of the lysosomal enzymes CTSD and CTSB in control and BD hiPSC-RPE. Bar = 20 µm. ACTN = ACTIN control. BD, Best disease; DAPI, 4′,6-diamidino-2-phenylindole; hiPSC, human induced pluripotent stem cell; RPE, retinal pigment epithelium.

24-hour time point, RHO levels in untreated control hiPSC-RPE were lower than in BafA1-treated control hiPSC-RPE (lane 3 versus lane 4). No difference in the levels of ACTIN (ACTN), a loading control, was observed between untreated and BafA1-treated hiPSC-RPE (**Figure 4a**).

We next sought to determine if POS breakdown could be enhanced in normal hiPSC-RPE with therapeutically relevant concentrations of VPA, an FDA-approved drug that has been shown to augment protein degradation.[39–44] After feeding cells with unlabeled POS as described above, RHO levels at 0 hours were higher in some 200 or 500 µmol/l VPA-treated hiPSC-RPE cultures compared to untreated control hiPSC-RPE, suggesting possible enhanced uptake of POS in the presence of VPA (**Figure 4b**, lanes 1–3). However, even with higher initial RHO content, RHO levels 24 hours after feeding were significantly lower in control hiPSC-RPE treated with 500 µmol/l VPA compared to untreated or 200 µmol/l VPA-treated control hiPSC-RPE (**Figure 4b**, lanes 4–6; **Figure 4d**). We also investigated whether VPA could counteract the effect of BafA1 treatment on the rate of RHO degradation in control hiPSC-RPE (**Figure 4c**). Consistent with results shown in **Figure 4a**, control hiPSC-RPE cells treated with BafA1 showed higher amounts of POS 24 hours after feeding compared to untreated hiPSC-RPE cells (lane 5 versus lane 4). VPA (500 µmol/l) treatment significantly reduced the negative effect of BafA1 on RHO degradation in control hiPSC-RPE cells (**Figure 4c**; lane 6 versus lane 5). Quantification of the effect of VPA and BafA1 on POS breakdown in control hiPSC-RPE, as measured by RHO levels at 24 hours relative to 0 hours, is shown in **Figure 4d**. These experiments indicate that the rate of POS processing in normal hiPSC-RPE can be modulated with drugs that affect intracellular protein degradation.

Regulation of POS degradation by pharmacological treatments in BEST1 mutant models

Although VPA could increase RHO degradation in untreated and BafA1-treated control hiPSC-RPE, it remained to be seen if drug treatment could similarly accelerate POS breakdown in RPE harboring mutations in BEST1. Ideally, an *in vivo* model is employed for such analyses; therefore, we first carried out studies to determine whether VPA can be used as an experimental treatment in a canine model of autosomal recessive bestrophinopathy.[45–47] Importantly, variation in age of onset, clinical manifestations, and disease progression have been observed in dogs with BEST1 mutations, similar to the inter- and intrafamilial variability in the phenotypic expression reported in BD patients.[48–50] Following a 3-week VPA dose-escalation trial (see **Supplementary Information** for details) that did not reveal any adverse effects related to VPA administration, a maximum dose of 120 mg/kg twice daily[51] was given to older R25X- or P463fs-affected dogs with established disease. After a 12-week trial, no changes in disease appearance and unaltered disease progression were observed (data not shown). In contrast, VPA treatment in younger BEST1 mutant dogs prior to ophthalmoscopically visible lesions (**Figure 5a**) retarded severity and progression of the disease (**Figure 5b,c**). Although all VPA-treated dogs developed BD symptoms, the disease was more advanced in the untreated group progressing to stage 3 (an early pseudohypopyon phase) in comparison to the VPA-treated eyes reaching only stage 2 (vitelliform; **Figure 5c**). To determine if adequate VPA blood levels were achieved, we ran pharmacokinetics studies in all VPA-treated dogs. While the mean VPA elimination half-life in humans is ~16 hours,[52] we confirmed a previously published study that the drug

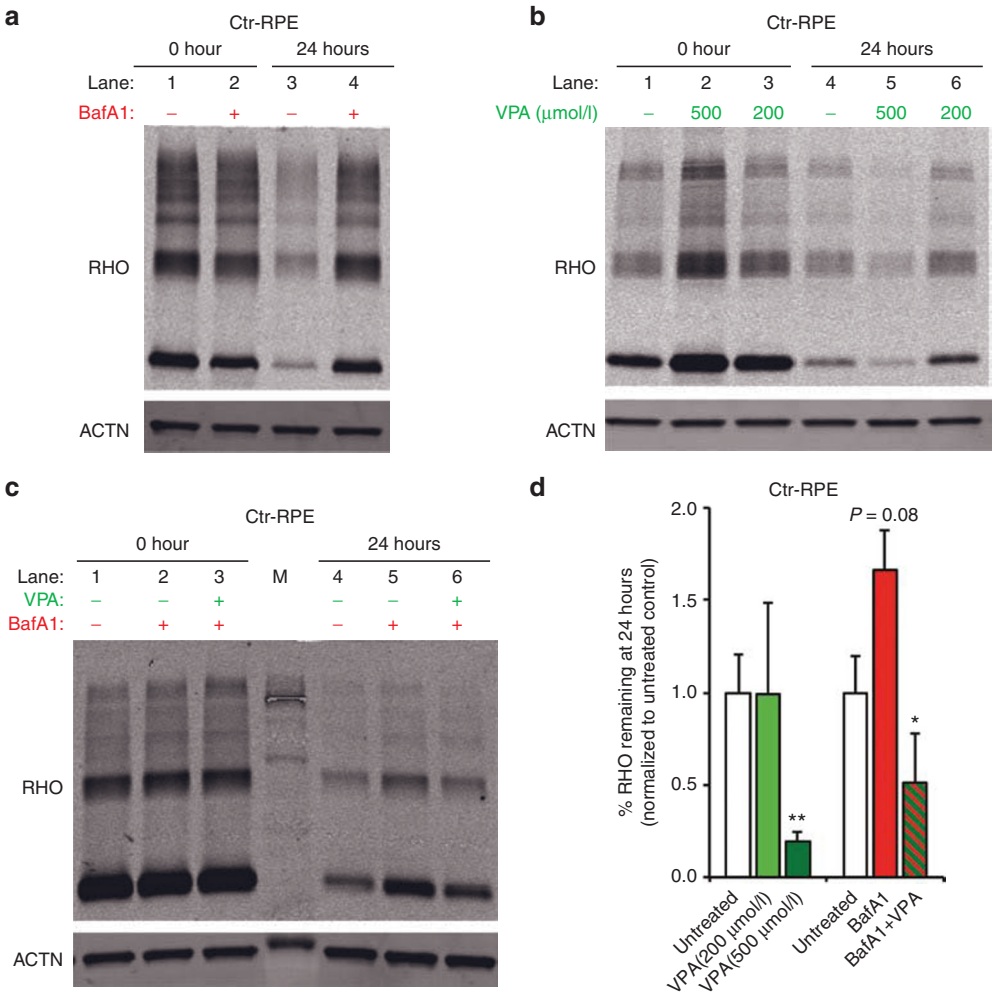

Figure 4 Pharmacological modulation of POS degradation in control hiPSC-RPE. (**a–c**) Representative western blot analyses showing the amount of the POS protein RHO present in control hiPSC-RPE at 0 and 24 hours after POS feeding in the presence or absence of drug. Drug treatments included bafilomycin (BafA1, 100 nmol/l) (**a**), valproic acid (VPA, 200 and 500 μmol/l) (**b**), and BafA1 (100 nmol/l) + VPA (500 μmol/l) (**c**). (**d**) Quantification of RHO levels 24 hours after POS feeding in control hiPSC-RPE (Ctr-1 + Ctr-2) treated with VPA (200 and 500 μmol/l), BafA1 (100 nmol/l), or VPA (500 μmol/l) + BafA1 (100 nmol/l). The percentage of RHO remaining at 24 hours relative to untreated control hiPSC-RPE is presented. ACTN = ACTIN control. *P < 0.05; **P < 0.01. hiPSC, human induced pluripotent stem cell; POS, photoreceptor outer segment; RHO, RHODOPSIN; RPE, retinal pigment epithelium.

is eliminated much more rapidly in dogs.[53] While we could consistently achieve therapeutic plasma levels in both adults and young dogs, these were not sustained, and fell to nontherapeutic levels within 4 hours (**Figure 6**). Higher VPA doses or more frequent dosing were not allowed due to concerns regarding drug toxicity in dogs.

Given the limitations of the canine bestrophiniopathy model, we returned to our hiPSC-RPE model to test the effects of VPA on POS degradation. We fed unlabeled POS to untreated and VPA-treated BD hiPSC-RPE cells for 2 hours and measured RHO levels at 0 and 24 hours after washing as described earlier. Degradation of RHO over this time period was greater in VPA-treated compared to untreated BD hiPSC-RPE (**Figure 7a**, 500 μmol/l VPA-treated: lane 2 versus lane 4, untreated: lane 1 versus lane 3). Although VPA could be acting through a variety of mechanisms, we found that VPA treatment increased autophagy after POS feeding as measured by the LC3 II/I ratio (**Supplementary Figure S6**). Therefore, in an attempt to augment the VPA effect, we exposed BD hiPSC-RPE to RAPA, an autophagy inducer,[28] both in the absence and presence of VPA. Treatment with either 100 nmol/l RAPA or 500 μmol/l VPA resulted in reduced RHO levels in POS-fed BD hiPSC-RPE at 24 hours (**Figure 7b**; VPA: 0.45 ± 0.09, P < 0.05, RAPA: 0.59 ± 0.09, P = 0.12). However, combinatorial therapy with 500 μmol/l VPA + 100 nmol/l RAPA caused a much greater reduction in RHO levels at 24 hours than either treatment alone (**Figure 7b**; 0.14 ± 0.04, P < 0.005). Of note, the synergistic effect of RAPA was not tested *in vivo*, as it is known to cause severe side effects in dogs.[54] Regardless, the ability to rescue the phenotype of delayed POS degradation in BD hiPSC-RPE with both VPA and RAPA provides further evidence that impaired proteolytic ability may contribute to the disease pathology.

Lastly, we next measured accumulation of autofluorescent material in BD and control hiPSC-RPE after chronic POS feeding with and without daily treatment with 500 μmol/l VPA. VPA decreased the amount of retained autofluorescent material after 1.5 months of POS feeding in BD hiPSC-RPE, but not in control hiPSC-RPE (**Figure 7c,d and Supplementary Figure S7a,b**). Of note, no autofluorescence accumulation was seen in BD or control

hiPSC-RPE cells in the absence of POS feeding (**Figure 7c** and **Supplementary Figure 7a**). Altogether, these data indicate that POS processing in BD hiPSC-RPE can be enhanced with drugs that act at least in part by increasing protein degradation.

DISCUSSION

Our results demonstrate that POS degradation can be augmented pharmacologically in control and BD hiPSC-RPE. We also show that the delayed POS degradation observed in BD hiPSC-RPE can be mimicked in control hiPSC-RPE by administering a proteolytic inhibitor, bafilomycin A1 (BafA1). In both BD hiPSC-RPE and control hiPSC-RPE treated with BafA1, the POS degradation defect can be rescued with VPA, an FDA-approved drug that has been shown to increase cellular proteolysis.[39–41] Daily VPA treatment also reduced accumulation of autofluorescent material in BD hiPSC-RPE after chronic POS feeding.

We further found that the combination of VPA and RAPA was considerably more effective at increasing the rate of POS degradation in BD hiPSC-RPE than VPA alone. The synergism observed between VPA and RAPA, two drugs that can increase proteolysis,[28,39–41] suggests a possible link between abnormal protein degradation and defective POS handling in BD hiPSC-RPE. Interestingly, animal studies have demonstrated that HDAC inhibitors, including VPA, are protective in some forms of retinal degeneration and after ischemic retinal and cardiac injury, with one proposed mechanism of action being induction of autophagy.[55–58] However, both VPA and RAPA are known to exhibit pleiotropic effects, so it remains possible that their influences on proteolytic pathways and POS degradation are indirect.

While this study primarily examined whether drugs could mitigate the development of cellular pathology in BD hiPSC-RPE, pharmacological intervention may also be of benefit in later stages of disease. While no improvement was seen in established retinal lesions after treatment of adult BEST1 mutant canines with VPA, the effects of the drug may have been dampened by its rapid clearance. Nevertheless, given the option, it is preferable to slow or halt disease progression rather than attempt to reverse chronic cell and/or tissue damage. The fact that VPA has a well-established safety profile[59] and is routinely used long term in pediatric and adult patients makes it a particularly attractive therapeutic for BD, a disease that is frequently diagnosed in childhood before significant vision loss occurs.[60,61] (By contrast, RAPA has a more prominent side effect profile and thus may not be an optimal adjunctive drug.[62]) In the present study, delayed disease progression was observed in a small cohort of BEST1 mutant canines who were treated early and continuously with VPA, even though the daily therapeutic window was brief. Given the observed effects of VPA in BD hiPSC-RPE and its known safety profile in humans, further investigation into its therapeutic value may be warranted despite the absence of a suitable *in vivo* efficacy model.

Impairment of protein degradation machinery can occur during normal aging and in MDDs,[10,63,64] where it correlates with the accumulation of partially digested POS in RPE cells.[1,3,38,64] Thus, our findings in BD hiPSC-RPE could result from general disturbances in proteolysis. Baseline examination of protein degradation pathways and exocytosis revealed a greater oxidized protein burden, decreased free-UB levels, and increased exocytosis in BD hiPSC-RPE. Both increased protein oxidation and decreased free-UB levels can be a consequence of dysfunctional or overtaxed proteolytic pathways, whereas increased exocytosis may be an adaptive response to the excess material within the cell.

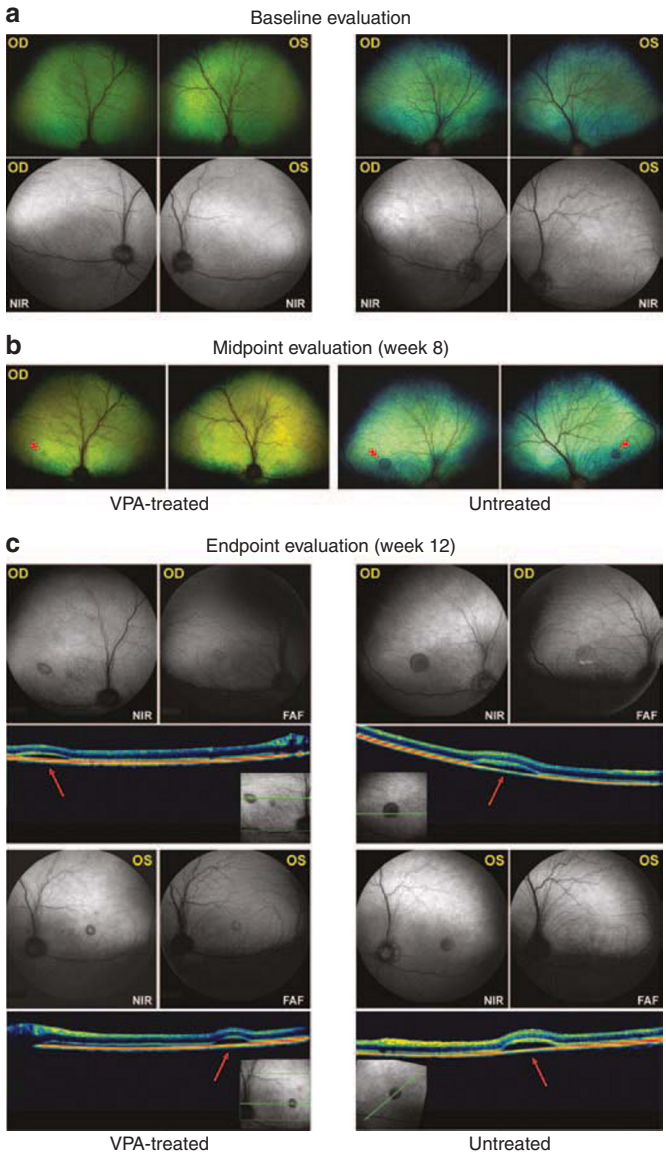

Figure 5 Evaluation of VPA treatment in the canine BEST1 mutant model. (**a**) Baseline ophthalmic and cSLO evaluations performed on two 3-month-old littermates affected with c.C73T/p.R25X mutation in the canine *BEST1* gene. (**b**) Clinical manifestation of BD symptoms documented during retinal exam 8 weeks post-VPA treatment (left panel: treated sibling) versus untreated sibling control (right panel). BD lesions limited to the canine fovea-like region[83] are denoted by arrowheads (red). (**c**) cSLO/SD-OCT endpoint evaluation of BD lesions (left panel: treated sibling) versus untreated sibling control (right panel). BD lesions are documented by *in vivo* imaging in NIR and FAF modes, and on the cross-sectional OCT scans (arrows). Note the autofluorescent debris accumulating in pseudohypopyon lesion (OD, FAF) of the untreated dog. BD, Best disease; cSLO, confocal scanning laser ophthalmoscopy; FAF, fundus autofluorescence; NIR, near-infrared; SD-OCT, spectral domain optical coherence tomography; OD, right eye; OS, left eye: applies to all panels; VPA, valproic acid.

While the function and localization of BEST-1 protein remain the topic of debate, recent publications of the X-ray crystal

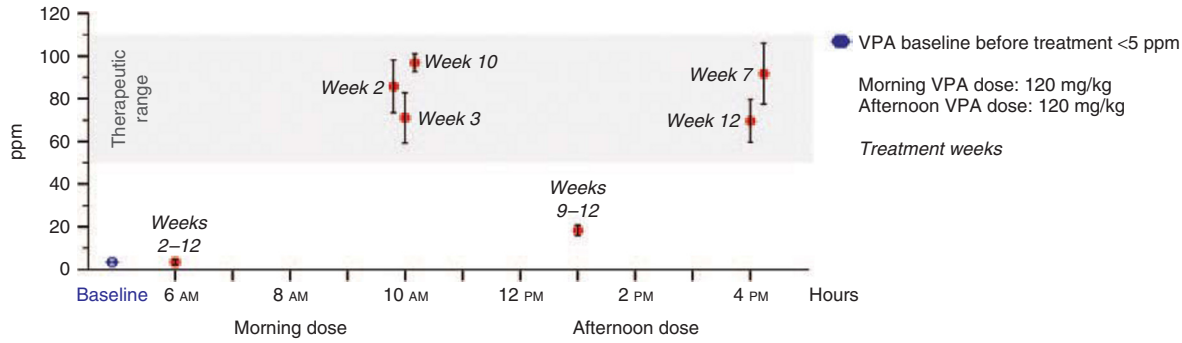

Figure 6 VPA pharmacokinetic profile during continued treatment in canine BEST1 mutant model. VPA serum levels were determined for all BD-affected (n = 4) and control (n = 1) dogs. Total plasma VPA concentrations reached therapeutic range within 2 hours postadministration of a single dose and rapidly declined within 3 hours thereafter (1 PM, weeks 9–12). Baseline (untreated) levels were present by the 6 AM time period of the day following dosing (weeks 2–12). The error bars represent SD of the measurements for n ≥ 3 per time point. BD, Best disease; VPA, valproic acid.

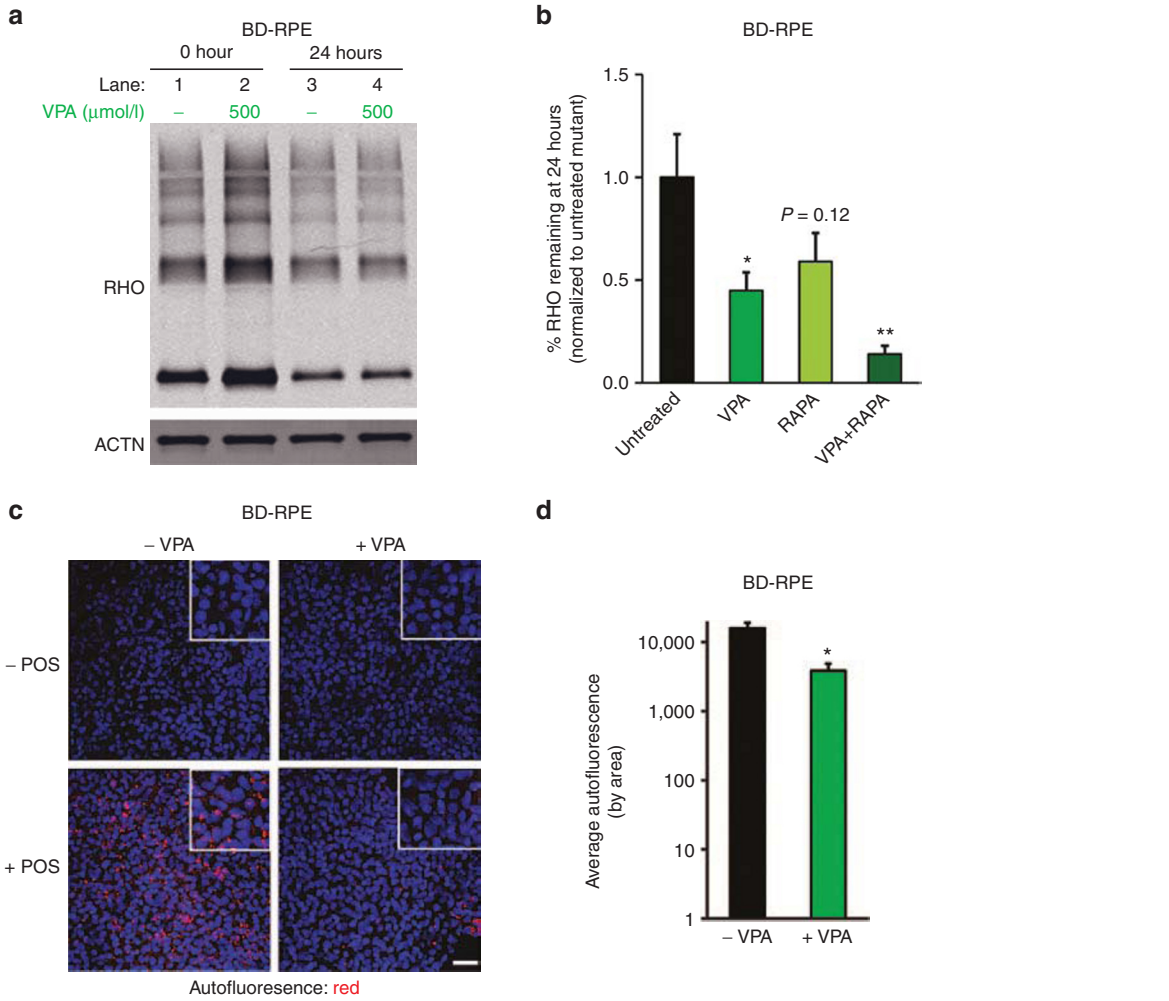

Figure 7 Pharmacological modulation of POS degradation in BD hiPSC-RPE. (**a**) Representative western blot analysis comparing the amount of the POS protein RHO in untreated and VPA-treated (500 µmol/l) BD hiPSC-RPE at 0 and 24 hours after POS feeding. (**b**) Quantification of RHO levels 24 hours after POS feeding in untreated versus treated (500 µmol/l VPA, 100 nmol/l RAPA, or 500 µmol/l VPA + 100 nmol/l RAPA) BD hiPSC-RPE (BD-1 + BD-2). (**c**) Confocal microscopic images showing accumulation of autofluorescent material (red channel) in untreated (left panels) and VPA-treated (500 µmol/l; right panels) BD-2 hiPSC-RPE in the presence (lower panels) or absence (upper panels) of daily POS feeding for 1.5 months. (**d**) Quantification of average autofluorescence levels in untreated and VPA-treated BD-2 hiPSC-RPE after daily POS feeding for 1.5 months (note log scale on y-axis). Bar = 50 µm. ACTN = ACTIN control. *P < 0.05; **P = 0.001. BD, Best disease; hiPSC, human induced pluripotent stem cell; POS, photoreceptor outer segment; RAPA, rapamycin; RHO, RHODOPSIN; RPE, retinal pigment epithelium; VPA, valproic acid.

structures of bacterial and avian Best-1 point to a role as a calcium-activated chloride channel.[65,66] Significant evidence also links BEST-1 to the trafficking of calcium from endoplasmic reticulum stores.[67,68] Therefore, the abnormalities in proteolysis and POS handling found in BD hiPSC-RPE may be secondary to subtle disturbances in cellular ion homeostasis. Along this line of reasoning, calcium is known to regulate POS processing,[69–71] and changes in calcium and chloride homeostasis can influence proteolytic pathways.[72–76]

A limitation of *in vitro* RPE models as systems to evaluate POS handling is that they do not replicate the intricacies of the photoreceptor–RPE complex *in vivo.* This shortcoming might have affected our ability to consistently document defects in binding and uptake of POS in BD hiPSC-RPE, although such effects were occasionally observed (**Figure 2a**).[2] Therefore, although delayed POS degradation appears to contribute to the BD hiPSC-RPE phenotype, other important effects on POS handling, such as phagocytosis, may have escaped definitive detection in our assays. Regardless, the finding that VPA can accelerate the clearance of ingested POS in hiPSC-RPE, with or without concurrent enhancement of POS uptake (**Figure 7a**), holds promise for its ability to beneficially affect the BD phenotype.

In summary, we have shown that modulating proteolytic machinery in BD and control hiPSC-RPE can influence the rate of POS degradation. Our findings have implications for drug-based therapy of BD and other MDDs that demonstrate accumulation of POS breakdown products in RPE. In addition, we call attention to a situation in which a hiPSC-based model may be preferable to available animal models for drug efficacy testing. A similar scenario recently arose during development of a gene therapy strategy for choroideremia, a rare inherited retinal degenerative disorder that also affects RPE.[77] Since no suitable animal model of choroideremia exists, efficacy was established exclusively using patient-specific hiPSCs, which led in part to approval for a clinical trial.

The utility of hiPSC models for screening pharmaceuticals is perhaps greatest for diseases like BD that display extensive genotype-phenotype heterogeneity.[48–50,78–80] Instead of searching for - or attempting to create - animal models for each pathogenic mutation (*e.g.*, BD has >100 known disease-causing mutations), hiPSCs can be made relatively quickly and inexpensively from individual patients, allowing direct clinical correlation and "personalized" drug testing. BD hiPSC-RPE models are also convenient platforms for high throughput drug screening, which could lead to combinatorial treatment approaches targeting other cellular pathways affected in this disease (*e.g.*, chloride and calcium homeostasis). However, there are clear disadvantages of *in vitro* systems for drug testing as well, including their inability to evaluate bioavailability or effects on vision. Thus, at minimum, safety and bio-distribution studies require use of appropriate animal models regardless of how efficacy is established.

MATERIALS AND METHODS

hiPSC production, passage, and differentiation to RPE fate. Fibroblasts obtained from skin biopsies were reprogrammed to obtain hiPSCs as previously described[2] whereupon they were maintained on either mouse embryonic feeder (MEF) feeder layers using our previously established protocol, or on Matrigel (WiCell, Madison, WI).[2,81] hiPSCs on Matrigel were cultured in commercially available TeSR media (Wicell), and any areas of spontaneous cellular differentiation were mechanically removed. hiPSCs were passaged every 3 to 4 days and differentiated to RPE as previously described.[2,81] Briefly, hiPSC colonies were lifted with dispase (2 mg/ml) and put in embryoid body medium (EBM) (DMEM/F12, 20% KOSR, 1% MEM nonessential amino acids, 1 mmol/l L-glutamine, and 0.1 mmol/l β-ME) to grow as suspended embryoid bodies (EBs). EBs were transitioned to neural induction medium (NIM) (DMEM/F12, 1% N2 supplement, MEM nonessential amino acids, and 2 μg/ml heparin) over days 1, 2, and 3 by introducing media containing EBM/NIM in ratios of 3:1, 1:1, and 1:3, respectively. By day 4, the media contained NIM alone. On day 7, suspended EB aggregates in NIM were plated onto laminin-coated culture plates to allow the EBs to attach to the culture plate; thereafter, cell aggregates were grown for an additional 10 days in NIM. On day 16, NIM was replaced with retinal differentiation medium (RDM) (DMEM/F12 (3:1), 2% B27 supplement (without retinoic acid), and penicillin streptomycin). Adherent cultures of cells in RDM were maintained until large patches of pigmented RPE cells appeared (~day 60–90). Pigmented RPE cell clusters were then manually dissected under a microoscope, dissociated with Trypsin-EDTA (0.05%), and plated onto extracellular matrix-coated transwell inserts (Corning Costar, Corning Incorporated, Corning, NY) in RDM + 10% FBS. The media was switched after 2 days to RDM + 2% FBS and cells were grown until confluent. After confluency was reached, cells were maintained in RDM to allow RPE cells to mature. Of note, hiPSC lines from two independent clones derived from each individual (Ctr-1, Ctr-2, BD-1, and BD-2) were used in this study.

Quantification of oxidized proteins. RPE cells were lysed in 1× phosphate-buffered saline (PBS) containing protease inhibitor cocktail (PI; Sigma, St Louis, MO). Protein samples thus obtained were treated with DNase I (Life Technologies, Grand Island, NY) and quantified using the Bio-Rad DC protein assay (Bio-Rad, Hercules, CA). Levels of oxidized proteins were evaluated using an ELISA kit for quantification of protein carbonyls (Cat. # STA 310; Cell Biolabs, San Diego, CA) according to manufacturer's instructions.

Quantitative RT-PCR. Total RNA was extracted using either the RNeasy Mini Plus Kit (Qiagen, Valencia, CA) or Arcturus PicoPure RNA Isolation Kit (Life Technologies), and cDNA was synthesized (iScript cDNA Synthesis Kit Biorad, Hercules, CA) according to manufacturer's instructions. Extracted RNA was subjected to DNase I treatment to remove any genomic DNA contamination prior to cDNA synthesis. Quantitative RT-PCR (qRT-PCR) experiments were carried out using cDNA samples, gene-specific primers (**Supplementary Table S2**), SsoAdvanced SYBR Green Supermix (Bio-Rad), and a Bio-Rad C1000 thermal cycler (40 cycles). Results were compiled and analyzed using Bio-Rad CFX software and Microsoft Excel.

Western blotting. Total protein was isolated by lysing cells in RIPA buffer (Pierce, Rockford, IL) containing protease inhibitor (PI) and quantified using a Biorad DC protein assay (Bio-Rad). Protein lysates (5–20 μg) were denatured in 1× Laemelli + 5% β-ME buffer and separated on either a 10, 12, or 4–20% Tris–Cl gradient gel. Proteins from the gel were transferred onto PVDF-licor membranes, stained with Ponceau, and incubated with blocking buffer (Licor Biosciences, Lincoln, NE) for 1 hour at room temperature. Membranes were then incubated overnight at 4 °C with the following primary antibodies: rabbit anti- LC3 (1:200; Novus Biologicals, Littleton, CO), mouse anti-SQSTM1 (also referred to as anti-P62) (1:400; Santa Cruz Biotechnology, Dallas, TX), mouse anti-LAMP1 (1:500; Santa Cruz Biotechnology), mouse anti-LAMP2 (1:500; Santa Cruz Biotechnology), goat anti-CTSD (1:500; Santa Cruz Biotechnology), goat anti-CTSB (1:500; Santa Cruz Biotechnology), rabbit anti-UB (1:1,000; Dako, Carpinteria, CA), rabbit anti-UB Lys63 (Millipore, Billerica, MA), rabbit anti-UB Lys48 (1:1,000; Millipore), mouse anti-CD63 (1:500; Novus Biologicals),

goat anti-APOE1 (1:500; Millipore), mouse anti-RHO (1:500; Millipore), and/or goat anti-ACTN (1:500; Santa Cruz Biotechnology). The following day, blots were washed four times in wash buffer (PBS + 0.1% tween) and incubated for 1 hour at room temperature in appropriate secondary antibodies (Licor Biosciences). Following incubation, blots were washed four times, and proteins were visualized on an Odyssey Infrared Imager (Licor). In most experiments, individual western blots were stripped (stripping buffer, LICOR) and probed up to three times with different primary antibodies. Of note, all quantitative analyses of the western blot data were carried out using image acquisition software (Licor Odyssey 3.0 and/or Image Studio).

Immunohistochemistry. hiPSC-RPE cells were washed in ice-cold PBS, fixed in 4% paraformaldehyde on ice for 30 minutes and incubated in blocking solution (10% normal donkey serum and 0.01% Triton X-100 in PBS) for 1 hour at room temperature. Cells were then incubated overnight at 4 °C in the following primary antibodies: rabbit anti-ZO-1 (1:100; Life Technologies), mouse anti-SQSTM1 (also referred to as anti-P62) (1:200; Santa Cruz Biotechnology), goat anti-CTSD (1:200; Santa Cruz), mouse anti- LAMP1 (1:200; Santa Cruz), rabbit anti-UB (1:150; Dako), and mouse anti-CD63 (1:200; Novus Biologicals). The next day, cells were washed three times in wash buffer (0.01% Triton X-100 in PBS) and incubated for 1 hour in Alexa-labeled secondary antibodies (1:500; Life Technologies). Cells were then stained with 4′,6-diamidino-2-phenylindole (DAPI) for 30 minutes, washed three times, and mounted using Prolong Gold (Life Technologies). Fluorescence imaging was carried out on a Nikon C1 and/or Nikon A1 confocal microscope (Nikon Instruments, Melville, NY).

Proteasome activity. Pigmented monolayers of hiPSC-RPE grown on transwells were dissociated with Trypsin-EDTA (0.05%) and the amount of chymotrypsin-like protease activity was measured using the Proteasome-Glo Chymotrypsin-Like cell-based assay (Promega, Madison, WI) in accordance with the manufacturer's instructions. Briefly, dissociated cells resuspended in PBS were incubated with a mixture of chymotrypsin-like assay substrate (Suc-LLVY-glo) and luciferase reagent for 30 minutes at room temperature. Thereafter, luminescence was measured using a Glomax luminometer (Promega).

Phagocytosis assay. hiPSC-RPE grown as pigmented monolayers on transwells were used for phagocytosis assays as previously described.[2] In brief, for each experiment, hiPSC-RPE cells from each treatment group were incubated with an equivalent amount of unlabeled bovine POS for 2 hours. Afterward, 1× PBS was used to vigorously wash hiPSC-RPE cells 4–5 times to remove any POS that remained on the surface of the transwell (designated as the 0 hour time point), and then the RPE was harvested for protein isolation. At 0, 4, 24, 48, and 120 hour time points after POS feeding and washing, hiPSC-RPE cells were washed an additional two times with 1× PBS. Isolated proteins were utilized in western blotting experiments and probed for the POS-specific protein, RHO. hiPSC-RPE cells that had not been POS-fed served as negative controls. Of note, hiPSC-RPE belonging to different treatment groups were fed POS at the same time (either in the morning or early afternoon), and all subsequent processing (e.g., washing, sample collection, protein isolation, and western blotting) for each group was performed in parallel. The bovine POS used in these experiments were isolated either in the lab using a previously described protocol[2] or obtained commercially (Invision Biosciences, Seattle, WA).

Lysosomal pH measurement. Pigmented monolayers of hiPSC-RPE and hfRPE cultured on transwells were employed for measurements of lysosomal pH using the commercially available dye, lysosensor yellow-blue (Life Technologies), as previously described.[82] The lysosome perturbation compound, chloroquine (100 µmol/l), was used as a positive control in these experiments.

Exosome isolation and quantification. For exosome isolation, mature monolayers of hiPSC-RPE grown on transwells were incubated in filtered RDM overnight. The next day, media was collected separately from the apical and basal compartments of the transwell chambers and replaced with fresh filtered RDM. PI was added to the collected media samples, which were immediately stored at −80 °C until analyzed further. Media collected daily from the apical and basal chambers for a total period of 15–30 days was used for exosome isolation by differential centrifugation. Briefly, media was centrifuged sequentially at 300 × g for 10 minutes, 2,000 × g for 10 minutes, and 10,000 × g for 30 minutes. After each centrifugation, supernatant was collected and the pellet containing cells and/or cellular debris was discarded. The final supernatant thus obtained was subjected to a final centrifugation at 100,000 × g for 60–75 minutes to pellet exosomes and contaminating proteins. Exosome samples were then washed 1× in PBS and re-centrifuged to obtain purified exosomes. Total protein was extracted from freshly isolated exosomes, quantified, and visualized via western blotting as described above. Of note, we validated our exosome isolation protocol by quantifying the amount of CD63, an exosome marker, in protein samples from cell lysates versus purified exosomes. Western blot analysis revealed higher levels of CD63 in exosome samples compared to equivalent whole cell lysate samples (**Supplementary** Figure S2B). Furthermore, we performed western analysis on undiluted versus diluted exosome samples to validate the use of the CD63 antibody for quantitative analysis (**Supplementary Figure S2B**).

VPA trial in canine BD model. All dogs were bred and maintained at the University of Pennsylvania Retinal Disease Studies Facility (RDSF), Kennett Square, Pennsylvania, and supported by facility grants from FFB and NEI/NIH EY06855. The studies were carried out in strict accordance with the recommendations in the Guide for the Care and Use of Laboratory Animals of the NIH, the USDA's Animal Welfare Act and Animal Welfare Regulations, and complied with the ARVO Statement for the Use of Animals in Ophthalmic and Vision Research. The protocol was approved by the Institutional Animal Care and Use Committee of the University of Pennsylvania (IACUC Protocol #803422). Adult (n = 2; 1 and 5 years) and young (n = 4; 3 months) dogs carrying homozygous c.C73T/p.R25X or c.1388delC/p.P463fs mutation in *BEST1* and a wild-type control (n = 1; 4 years of age) were used. Both mutations result in identical disease phenotype and progression.[45,46] Dogs were treated with an oral solution of VPA (Pharmaceutical Assoc, Greenville, SC) administered twice daily, receiving doses of 30- (week 1), 60- (week 2), or 120 mg/kg (week 3) during the dose-escalation study conducted on two adult affected and the wild-type control, and continued at 120 mg/kg twice daily for the next 12 weeks.[51] Blood samples were collected prior to VPA trial, and then every week during the VPA treatment at selected time points. Evaluation of VPA plasma levels was performed by the Diagnostic Center for Population and Animal Health at Michigan State University, East Lansing, Michigan. Ophthalmic examinations, including biomicroscopy, indirect ophthalmoscopy, and fundus photography, were conducted on a weekly basis. Noninvasive *en face* and cross-sectional imaging using confocal scanning laser ophthalmoscopy and spectral domain optical coherence tomography (SD-OCT) was performed under general anesthesia as described previously[47,83] prior to and after completion of the study. Post-acquisition processing of OCT data was performed on Heidelberg Eye Explorer software (version 1.7.0.0; Heidelberg Engineering GmbH, Heidelberg, Germany).

Statistics. Data are expressed as mean ± SEM and compared using Student's t-test. Data in specific experiments were subjected to F-test to determine the appropriate Student's t-test parameters. Significance was assigned for P values less than 0.05. Of note, in **Figure 4**, significance for VPA + BafA1 was determined by Student's t-test against the BafA1-treated group, and in **Figure 7**, data were normalized to the percentage of RHO remaining at 24 hours in untreated BD hiPSC-RPE. All hiPSC-RPE experiments were performed on n ≥ 3 independent cultures with the exception of the chronic (>1–2 month) POS feeding experiments ± VPA treatment, in which two independent hiPSC-differentiation runs were performed with 2–3 separate samples per condition (untreated, VPA only, POS only, and POS + VPA).

SUPPLEMENTARY MATERIAL

Figure S1. Autofluorescence accumulation and RHO degradation in control vs. BD hiPSC-RPE.

Figure S2. Proteasomal activity and quantification of free-UB and poly-UB in control vs. BD hiPSC-RPE.

Figure S3. Comparison of CD63 localization and exosome protein levels in control and BD hiPSC-RPE.

Figure S4. Localization and expression of autophagy and lysosomal proteins and quantification of lysosomal pH in control vs. BD hiPSC-RPE.

Figure S5. Quantitative analysis of autophagy and lysosomal protein expression in control vs. BD hiPSC-RPE.

Figure S6. Comparison of LC3 II/I ratios in POS-fed BD hiPSC-RPE with and without VPA treatment.

Figure S7. Autofluorescence accumulation in untreated vs. VPA-treated control hiPSC-RPE after chronic POS feeding.

Table S1. Normalized fold expression in BD hiPSC-RPE relative to unaffected sibling control hiPSC-RPE.

Table S2. Primers used for amplifying oxidative stress genes.

ACKNOWLEDGMENTS

We thank Aparna Lakkaraju (University of Wisconsin, Madison) for her input and advice on lysosomal pH measurements and other biochemical assays used in this study. This work was supported by the Macula Vision Research Foundation, the Foundation Fighting Blindness, NIH R01 EY021218, NIH P30 HD03352, the Muskingum County Community Foundation, the Reeves Foundation, the Retina Research Foundation (RRF) Emmett A. Humble Distinguished Directorship, and the Sandra Lemke Trout Chair in Eye Research (to D.M.G.), and an RRF Pilot Study Grant (to R.S.).

REFERENCES

1. Wavre-Shapton, ST, Tolmachova, T, Lopes da Silva, M, da Silva, M, Futter, CE and Seabra, MC (2013). Conditional ablation of the choroideremia gene causes age-related changes in mouse retinal pigment epithelium. *PLoS One* **8**: e57769.
2. Singh, R, Shen, W, Kuai, D, Martin, JM, Guo, X, Smith, MA *et al.* (2013). iPS cell modeling of Best disease: insights into the pathophysiology of an inherited macular degeneration. *Hum Mol Genet* **22**: 593–607.
3. Sparrow, JR and Boulton, M (2005). RPE lipofuscin and its role in retinal pathobiology. *Exp Eye Res* **80**: 595–606.
4. Krohne, TU, Kaemmerer, E, Holz, FG and Kopitz, J (2010). Lipid peroxidation products reduce lysosomal protease activities in human retinal pigment epithelial cells via two different mechanisms of action. *Exp Eye Res* **90**: 261–266.
5. Bosch, E, Horwitz, J and Bok, D (1993). Phagocytosis of outer segments by retinal pigment epithelium: phagosome-lysosome interaction. *J Histochem Cytochem* **41**: 253–263.
6. Deguchi, J, Yamamoto, A, Yoshimori, T, Sugasawa, K, Moriyama, Y, Futai, M *et al.* (1994). Acidification of phagosomes and degradation of rod outer segments in rat retinal pigment epithelium. *Invest Ophthalmol Vis Sci* **35**: 568–579.
7. Kim, JY, Zhao, H, Martinez, J, Doggett, TA, Kolesnikov, AV, Tang, PH *et al.* (2013). Noncanonical autophagy promotes the visual cycle. *Cell* **154**: 365–376.
8. Kaarniranta, K, Hyttinen, J, Ryhanen, T, Viiri, J, Paimela, T, Toropainen, E *et al.* (2010). Mechanisms of protein aggregation in the retinal pigment epithelial cells. *Front Biosci (Elite Ed)* **2**: 1374–1384.
9. Wang, AL, Lukas, TJ, Yuan, M, Du, N, Tso, MO and Neufeld, AH (2009). Autophagy and exosomes in the aged retinal pigment epithelium: possible relevance to drusen formation and age-related macular degeneration. *PLoS One* **4**: e4160.
10. Shang, F and Taylor, A (2012). Roles for the ubiquitin-proteasome pathway in protein quality control and signaling in the retina: implications in the pathogenesis of age-related macular degeneration. *Mol Aspects Med* **33**: 446–466.
11. Ramos de Carvalho JE, Klaassen I, Vogels IM, Schipper-Krom S, van Noorden CJ, Reits E *et al.* (2013). Complement factor C3a alters proteasome function in human RPE cells and in an animal model of age-related RPE degeneration. *Invest Ophthalmol Vis Sci* **54**: 6489–6501.
12. Huang, LZ, Li, YJ, Xie, XF, Zhang, JJ, Cheng, CY, Yamashiro, K *et al.* (2015). Whole-exome sequencing implicates UBE3D in age-related macular degeneration in East Asian populations. *Nat Commun* **6**: 6687.
13. Ramkumar, HL, Zhang, J and Chan, CC (2010). Retinal ultrastructure of murine models of dry age-related macular degeneration (AMD). *Prog Retin Eye Res* **29**: 169–190.
14. Mitter, SK, Song, C, Qi, X, Mao, H, Rao, H, Akin, D *et al.* (2014). Dysregulated autophagy in the RPE is associated with increased susceptibility to oxidative stress and AMD. *Autophagy* **10**: 1989–2005.
15. Guha, S, Liu, J, Baltazar, G, Laties, AM and Mitchell, CH (2014). Rescue of compromised lysosomes enhances degradation of photoreceptor outer segments and reduces lipofuscin-like autofluorescence in retinal pigmented epithelial cells. *Adv Exp Med Biol* **801**: 105–111.
16. Singh, R, Phillips, MJ, Kuai, D, Meyer, J, Martin, JM, Smith, MA *et al.* (2013). Functional analysis of serially expanded human iPS cell-derived RPE cultures. *Invest Ophthalmol Vis Sci* **54**: 6767–6778.
17. Kokkinaki, M, Sahibzada, N and Golestaneh, N (2011). Human induced pluripotent stem-derived retinal pigment epithelium (RPE) cells exhibit ion transport, membrane potential, polarized vascular endothelial growth factor secretion, and gene expression pattern similar to native RPE. *Stem Cells* **29**: 825–835.
18. Croze, RH and Clegg, DO (2014). Differentiation of pluripotent stem cells into retinal pigmented epithelium. *Dev Ophthalmol* **53**: 81–96.
19. Buchholz, DE, Hikita, ST, Rowland, TJ, Friedrich, AM, Hinman, CR, Johnson, LV *et al.* (2009). Derivation of functional retinal pigmented epithelium from induced pluripotent stem cells. *Stem Cells* **27**: 2427–2434.
20. Buchholz, DE, Pennington, BO, Croze, RH, Hinman, CR, Coffey, PJ and Clegg, DO (2013). Rapid and efficient directed differentiation of human pluripotent stem cells into retinal pigmented epithelium. *Stem Cells Transl Med* **2**: 384–393.
21. Maruotti, J, Wahlin, K, Gorrell, D, Bhutto, I, Lutty, G and Zack, DJ (2013). A simple and scalable process for the differentiation of retinal pigment epithelium from human pluripotent stem cells. *Stem Cells Transl Med* **2**: 341–354.
22. Westenskow, PD, Kurihara, T and Friedlander, M (2014). Utilizing stem cell-derived RPE cells as a therapeutic intervention for age-related macular degeneration. *Adv Exp Med Biol* **801**: 323–329.
23. Ferrer, M, Corneo, B, Davis, J, Wan, Q, Miyagishima, KJ, King, R *et al.* (2014). A multiplex high-throughput gene expression assay to simultaneously detect disease and functional markers in induced pluripotent stem cell-derived retinal pigment epithelium. *Stem Cells Transl Med* **3**: 911–922.
24. Kamao, H, Mandai, M, Okamoto, S, Sakai, N, Suga, A, Sugita, S *et al.* (2014). Characterization of human induced pluripotent stem cell-derived retinal pigment epithelium cell sheets aiming for clinical application. *Stem Cell Reports* **2**: 205–218.
25. Brandl, C, Zimmermann, SJ, Milenkovic, VM, Rosendahl, SM, Grassmann, F, Milenkovic, A *et al.* (2014). In-depth characterisation of Retinal Pigment Epithelium (RPE) cells derived from human induced pluripotent stem cells (hiPSC). *Neuromolecular Med* **16**: 551–564.
26. Yamamoto, A, Tagawa, Y, Yoshimori, T, Moriyama, Y, Masaki, R and Tashiro, Y (1998). Bafilomycin A1 prevents maturation of autophagic vacuoles by inhibiting fusion between autophagosomes and lysosomes in rat hepatoma cell line, H-4-II-E cells. *Cell Struct Funct* **23**: 33–42.
27. Jahreiss, L, Menzies, FM and Rubinsztein, DC (2008). The itinerary of autophagosomes: from peripheral formation to kiss-and-run fusion with lysosomes. *Traffic* **9**: 574–587.
28. Nair, S and Ren, J (2012). Autophagy and cardiovascular aging: lesson learned from rapamycin. *Cell Cycle* **11**: 2092–2099.
29. Szweda, PA, Camouse, M, Lundberg, KC, Oberley, TD and Szweda, LI (2003). Aging, lipofuscin formation, and free radical-mediated inhibition of cellular proteolytic systems. *Ageing Res Rev* **2**: 383–405.
30. Blasiak, J, Petrovski, G, Veréb, Z, Facskó, A and Kaarniranta, K (2014). Oxidative stress, hypoxia, and autophagy in the neovascular processes of age-related macular degeneration. *Biomed Res Int* **2014**: 768026.
31. Campello, L, Esteve-Rudd, J, Cuenca, N and Martín-Nieto, J (2013). The ubiquitin-proteasome system in retinal health and disease. *Mol Neurobiol* **47**: 790–810.
32. Höhn, A, König, J and Grune, T (2013). Protein oxidation in aging and the removal of oxidized proteins. *J Proteomics* **92**: 132–159.
33. Jung, T, Höhn, A and Grune, T (2013). The proteasome and the degradation of oxidized proteins: Part II - protein oxidation and proteasomal degradation. *Redox Biol* (epub ahead of print).
34. Wang, AL, Lukas, TJ, Yuan, M, Du, N, Tso, MO and Neufeld, AH (2009). Autophagy, exosomes and drusen formation in age-related macular degeneration. *Autophagy* **5**: 563–564.
35. Shaid, S, Brandts, CH, Serve, H and Dikic, I (2013). Ubiquitination and selective autophagy. *Cell Death Differ* **20**: 21–30.
36. Ferguson, TA and Green, DR (2014). Autophagy and phagocytosis converge for better vision. *Autophagy* **10**: 165–167.
37. Rakoczy, PE, Lai, CM, Baines, M, Di Grandi, S, Fitton, JH and Constable, IJ (1997). Modulation of cathepsin D activity in retinal pigment epithelial cells. *Biochem J* **324**: 935–940.
38. Zhang, D, Lai, MC, Constable, IJ and Rakoczy, PE (2002). A model for a blinding eye disease of the aged. *Biogerontology* **3**: 61–66.
39. Wang, D, Fang, C, Zong, NC, Liem, DA, Cadeiras, M, Scruggs, SB *et al.* (2013). Regulation of acetylation restores proteolytic function of diseased myocardium in mouse and human. *Mol Cell Proteomics* **12**: 3793–3802.
40. Yoon, JY, Szwajcer, D, Ishdorj, G, Benjaminson, P, Xiao, W, Kumar, R *et al.* (2013). Synergistic apoptotic response between valproic acid and fludarabine in chronic lymphocytic leukaemia (CLL) cells involves the lysosomal protease cathepsin B. *Blood Cancer J* **3**: e153.
41. Xiong, N, Jia, M, Chen, C, Xiong, J, Zhang, Z, Huang, J *et al.* (2011). Potential autophagy enhancers attenuate rotenone-induced toxicity in SH-SY5Y. *Neuroscience* **199**: 292–302.
42. Davis, GE and Senger, DR (2005). Endothelial extracellular matrix: biosynthesis, remodeling, and functions during vascular morphogenesis and neovessel stabilization. *Circ Res* **97**: 1093–1107.
43. Centorrino, F, Kelleher, JP, Berry, JM, Salvatore, P, Eakin, M, Fogarty, KV *et al.* (2003). Pilot comparison of extended-release and standard preparations of divalproex sodium in patients with bipolar and schizoaffective disorders. *Am J Psychiatry* **160**: 1348–1350.
44. Cerveny, L, Svecova, L, Anzenbacherova, E, Vrzal, R, Staud, F, Dvorak, Z *et al.* (2007). Valproic acid induces CYP3A4 and MDR1 gene expression by activation of constitutive androstane receptor and pregnane X receptor pathways. *Drug Metab Dispos* **35**: 1032–1041.
45. Guziewicz, KE, Zangerl, B, Lindauer, SJ, Mullins, RF, Sandmeyer, LS, Grahn, BH *et al.* (2007). Bestrophin gene mutations cause canine multifocal retinopathy: a novel animal model for best disease. *Invest Ophthalmol Vis Sci* **48**: 1959–1967.

46. Zangerl, B, Wickström, K, Slavik, J, Lindauer, SJ, Ahonen, S, Schelling, C *et al.* (2010). Assessment of canine BEST1 variations identifies new mutations and establishes an independent bestrophinopathy model (cmr3). *Mol Vis* **16**: 2791–2804.
47. Guziewicz, KE, Zangerl, B, Komáromy, AM, Iwabe, S, Chiodo, VA, Boye, SL *et al.* (2013). Recombinant AAV-mediated BEST1 transfer to the retinal pigment epithelium: analysis of serotype-dependent retinal effects. *PLoS One* **8**: e75666.
48. Lacassagne, E, Dhuez, A, Rigaudière, F, Dansault, A, Vêtu, C, Bigot, K *et al.* (2011). Phenotypic variability in a French family with a novel mutation in the BEST1 gene causing multifocal best vitelliform macular dystrophy. *Mol Vis* **17**: 309–322.
49. Ponjavic, V, Eksandh, L, Andréasson, S, Sjöström, K, Bakall, B, Ingvast, S *et al.* (1999). Clinical expression of Best's vitelliform macular dystrophy in Swedish families with mutations in the bestrophin gene. *Ophthalmic Genet* **20**: 251–257.
50. Sohn, EH, Francis, PJ, Duncan, JL, Weleber, RG, Saperstein, DA, Farrell, DF *et al.* (2009). Phenotypic variability due to a novel Glu292Lys variation in exon 8 of the BEST1 gene causing best macular dystrophy. *Arch Ophthalmol* **127**: 913–920.
51. Wittenburg, LA, Bisson, L, Rose, BJ, Korch, C and Thamm, DH (2011). The histone deacetylase inhibitor valproic acid sensitizes human and canine osteosarcoma to doxorubicin. *Cancer Chemother Pharmacol* **67**: 83–92.
52. Keck, PE Jr and McElroy, SL (2002). Clinical pharmacodynamics and pharmacokinetics of antimanic and mood-stabilizing medications. *J Clin Psychiatry* **63** (suppl. 4): 3–11.
53. Löscher, W (1981). Plasma levels of valproic acid and its metabolites during continued treatment in dogs. *J Vet Pharmacol Ther* **4**: 111–119.
54. Stepkowski, SM, Tian, L, Wang, ME, Qu, X, Napoli, K and Kahan, BD (1997). Sirolimus in transplantation. *Arch Immunol Ther Exp (Warsz)* **45**: 383–390.
55. Alsarraf, O, Fan, J, Dahrouj, M, Chou, CJ, Menick, DR and Crosson, CE (2014). Acetylation: a lysine modification with neuroprotective effects in ischemic retinal degeneration. *Exp Eye Res* **127**: 124–131.
56. Koriyama, Y, Sugitani, K, Ogai, K and Kato, S (2014). Heat shock protein 70 induction by valproic acid delays photoreceptor cell death by N-methyl-N-nitrosourea in mice. *J Neurochem* **130**: 707–719.
57. Mockel, A, Obringer, C, Hakvoort, TB, Seeliger, M, Lamers, WH, Stoetzel, C *et al.* (2012). Pharmacological modulation of the retinal unfolded protein response in Bardet-Biedl syndrome reduces apoptosis and preserves light detection ability. *J Biol Chem* **287**: 37483–37494.
58. Xie, M, Kong, Y, Tan, W, May, H, Battiprolu, PK, Pedrozo, Z *et al.* (2014). Histone deacetylase inhibition blunts ischemia/reperfusion injury by inducing cardiomyocyte autophagy. *Circulation* **129**: 1139–1151.
59. Nalivaeva, NN, Belyaev, ND and Turner, AJ (2009). Sodium valproate: an old drug with new roles. *Trends Pharmacol Sci* **30**: 509–514.
60. Blodi, CF and Stone, EM (1990). Best's vitelliform dystrophy. *Ophthalmic Paediatr Genet* **11**: 49–59.
61. Michaelides, M, Hunt, DM and Moore, AT (2003). The genetics of inherited macular dystrophies. *J Med Genet* **40**: 641–650.
62. Sankhala, K, Mita, A, Kelly, K, Mahalingam, D, Giles, F and Mita, M (2009). The emerging safety profile of mTOR inhibitors, a novel class of anticancer agents. *Target Oncol* **4**: 135–142.
63. Li, Y, Wang, YS, Shen, XF, Hui, YN, Han, J, Zhao, W *et al.* (2008). Alterations of activity and intracellular distribution of the 20S proteasome in ageing retinal pigment epithelial cells. *Exp Gerontol* **43**: 1114–1122.
64. Guha, S, Baltazar, GC, Coffey, EE, Tu, LA, Lim, JC, Beckel, JM *et al.* (2013). Lysosomal alkalinization, lipid oxidation, and reduced phagosome clearance triggered by activation of the P2X7 receptor. *FASEB J* **27**: 4500–4509.
65. Kane Dickson, V, Pedi, L and Long, SB (2014). Structure and insights into the function of a Ca(2+)-activated Cl(-) channel. *Nature* **516**: 213–218.
66. Yang, T, Liu, Q, Kloss, B, Bruni, R, Kalathur, RC, Guo, Y *et al.* (2014). Structure and selectivity in bestrophin ion channels. *Science* **346**: 355–359.
67. Strauss, O, Neussert, R, Müller, C and Milenkovic, VM (2012). A potential cytosolic function of bestrophin-1. *Adv Exp Med Biol* **723**: 603–610.
68. Neussert, R, Müller, C, Milenkovic, VM and Strauss, O (2010). The presence of bestrophin-1 modulates the Ca2+ recruitment from Ca2+ stores in the ER. *Pflugers Arch* **460**: 163–175.
69. Zhang, L, Hui, YN, Wang, YS, Ma, JX, Wang, JB and Ma, LN (2011). Calcium overload is associated with lipofuscin formation in human retinal pigment epithelial cells fed with photoreceptor outer segments. *Eye (Lond)* **25**: 519–527.
70. Müller, C, Más Gómez, N, Ruth, P and Strauss, O (2014). CaV1.3 L-type channels, maxiK Ca(2+)-dependent K(+) channels and bestrophin-1 regulate rhythmic photoreceptor outer segment phagocytosis by retinal pigment epithelial cells. *Cell Signal* **26**: 968–978.
71. Karl, MO, Kroeger, W, Wimmers, S, Milenkovic, VM, Valtink, M, Engelmann, K *et al.* (2008). Endogenous Gas6 and Ca2+ -channel activation modulate phagocytosis by retinal pigment epithelium. *Cell Signal* **20**: 1159–1168.
72. Hosogi, S, Kusuzaki, K, Inui, T, Wang, X and Marunaka, Y (2014). Cytosolic chloride ion is a key factor in lysosomal acidification and function of autophagy in human gastric cancer cell. *J Cell Mol Med* **18**: 1124–1133.
73. Wartosch, L and Stauber, T (2010). A role for chloride transport in lysosomal protein degradation. *Autophagy* **6**: 158–159.
74. Liu, J, Lu, W, Guha, S, Baltazar, GC, Coffey, EE, Laties, AM *et al.* (2012). Cystic fibrosis transmembrane conductance regulator contributes to reacidification of alkalinized lysosomes in RPE cells. *Am J Physiol Cell Physiol* **303**: C160–C169.
75. East, DA and Campanella, M (2013). Ca2+ in quality control: an unresolved riddle critical to autophagy and mitophagy. *Autophagy* **9**: 1710–1719.
76. Decuypere, JP, Bultynck, G and Parys, JB (2011). A dual role for Ca(2+) in autophagy regulation. *Cell Calcium* **50**: 242–250.
77. Vasireddy, V, Mills, JA, Gaddameedi, R, Basner-Tschakarjan, E, Kohnke, M, Black, AD *et al.* (2013). AAV-mediated gene therapy for choroideremia: preclinical studies in personalized models. *PLoS One* **8**: e61396.
78. Johnson, AA, Lee, YS, Stanton, JB, Yu, K, Hartzell, CH, Marmorstein, LY *et al.* (2013). Differential effects of Best disease causing missense mutations on bestrophin-1 trafficking. *Hum Mol Genet* **22**: 4688–4697.
79. Johnson, AA, Lee, YS, Chadburn, AJ, Tammaro, P, Manson, FD, Marmorstein, LY *et al.* (2014). Disease-causing mutations associated with four bestrophinopathies exhibit disparate effects on the localization, but not the oligomerization, of Bestrophin-1. *Exp Eye Res* **121**: 74–85.
80. Boon, CJ, Klevering, BJ, Leroy, BP, Hoyng, CB, Keunen, JE and den Hollander, AI (2009). The spectrum of ocular phenotypes caused by mutations in the BEST1 gene. *Prog Retin Eye Res* **28**: 187–205.
81. Meyer, JS, Shearer, RL, Capowski, EE, Wright, LS, Wallace, KA, McMillan, EL *et al.* (2009). Modeling early retinal development with human embryonic and induced pluripotent stem cells. *Proc Natl Acad Sci U S A* **106**: 16698–16703.
82. Lakkaraju, A, Finnemann, SC and Rodriguez-Boulan, E (2007). The lipofuscin fluorophore A2E perturbs cholesterol metabolism in retinal pigment epithelial cells. *Proc Natl Acad Sci U S A* **104**: 11026–11031.
83. Beltran, WA, Cideciyan, AV, Guziewicz, KE, Iwabe, S, Swider, M, Scott, EM *et al.* (2014). Canine retina has a primate fovea-like bouquet of cone photoreceptors which is affected by inherited macular degenerations. *PLoS One* **9**: e90390.